Shahid Beheshti University

Researches in Earth Sciences

Journal homepage: https://esrj.sbu.ac.ir

Research Article

Landslide risk assessment: A case study of Varvasht Watershed, Lorestan province, Iran

Taher Farhadinejad[1*], Ebrahim Karimi Sangchini[1]

1-Soil Conservation and Watershed Management Research Department, Lorestan Agricultural and Natural Resources Research and Education Center(AREEO), Khorramabad, Iran

Received: 30 Apr 2026 Accepted: 12 Jul 2026

Abstract

Landslides represent one of the most destructive natural hazards worldwide, causing substantial economic losses and human casualties annually. The present study aims to address existing gaps by conducting a comprehensive landslide risk assessment in the Varvasht Watershed, Lorestan Province, Iran, using three machine learning models. The Varvasht Watershed is located in northwest Lorestan Provinces. A landslide inventory map was prepared based on 163 landslide polygons systematically surveyed and recorded. Seventeen conditioning factors were selected as independent variables influencing landslide occurrence. The dataset was randomly split into training (70% of the data) and validation (30% of the data) subsets to ensure unbiased model evaluation. Three machine learning models such as Support Vector Machine (SVM), Generalized Linear Model (GLM) and Artificial Neural Network (ANN) were employed. All models were validated using ROC curves. Vulnerability scoring was conducted by integrating the inherent value of elements with hazard classes. The final risk map was produced using the risk equation. Validation results demonstrated that the SVM model achieved the best performance with an AUC of 0.913. According to the SVM model, approximately 12.68% as high, and 11.94% as very high susceptibility. The final risk map revealed that approximately 19% of the area (equivalent to 2,968 hectares) is classified as high and very high-risk classes, necessitating prioritization in management and mitigation measures. The results of this study can serve as a scientific basis for land use planning, sustainable development, and landslide risk mitigation in the mountainous regions of Iran.

Keywords: Landslide risk assessment, Support Vector Machine (SVM), Artificial Neural Network (ANN), Generalized Linear Model (GLM), Varosht Watershed, Iran.

Citation: Farhadinejad, T. and Karimi Sangchini, E., 2026. Landslide risk assessment: A case study of Varvasht Watershed, Lorestan Province, Iran, *Res. Earth. Sci:* 17(3), (1-17) DOI: 10.48308/esrj.2026.107462

* Corresponding author E-mail address: E.karimi64@gmail.com

Introduction

Natural hazards and their consequent disasters have always posed significant challenges to human societies worldwide. Phenomena such as earthquakes, volcanic eruptions, tsunamis, cloud bursts, floods, and soil erosion are among the most destructive natural events (Oh and Lee, 2017; Arabameri et al, 2020a; Karimi Sangchini et al, 2026). Among these, landslides are recognized as one of the most frequent and destructive types of natural hazards, causing substantial economic losses and human casualties on an annual basis (Kelarestaghi and Ahmadi, 2009; Karimi Sangchini et al, 2022). The damaging impacts of landslides include the destruction of forests, fertile agricultural lands, residential areas, communication networks, and tourism infrastructure. Furthermore, landslides contribute to severe geomorphic and topographical modifications, which in turn may trigger secondary hazards such as flooding in hilly regions and tsunamis in coastal zones (Pham et al, 2019). Given the increasing frequency and intensity of landslide events, especially in mountainous regions, landslide susceptibility mapping has become a critical step in reducing associated damages (Aleotti and Chowdhury, 1999; Regmi et al, 2013; Karimi Sangchini et al, 2016). Iran, due to its unique physiographic, environmental, and climatic conditions, coupled with anthropogenic pressures and growing demands on natural resources, is highly vulnerable to landslide occurrences, particularly in its northern mountainous areas (Karimi Sangchini et al, 2011; Aghda et al, 2018). The country experiences various natural threats, including severe soil erosion through gully development, devastating floods, and destructive landslides, which have collectively resulted in approximately 500 billion IRR in financial damages (Arabameri et al, 2020b). Consequently, landslides have become a national disaster in Iran, necessitating systematic approaches to assessment and management. No universally accepted method exists for landslide susceptibility mapping, owing to the wide range of influencing factors and local environmental conditions (Chen et al, 2017a; Rahmati et al, 2018; Pourqasmi and Rahmati, 2018). However, the application of logical and quantitative approaches, including statistical and machine learning models, has significantly improved the accuracy and reliability of landslide zoning maps (Carrara et al, 2003; Dahal et al, 2008; Bathrellos et al, 2009; Kayastha et al, 2013; Karimi Sangchini et al, 2014). In recent years, data mining and machine learning techniques have gained widespread attention due to their high predictive accuracy and robust information processing capabilities.

Among these, Artificial Neural Networks (ANN) have been successfully applied in landslide susceptibility studies (Chen et al, 2017a; Harmouzi et al, 2019; Yao et al, 2022). Logistic Regression (GLM) has also been widely used as a generalized linear model for establishing relationships between landslide occurrences and environmental factors (Hong et al, 2015; Karimi Sangchini et al, 2016; Abedini et al, 2017; Hemasinghe et al, 2018; Shano et al, 2021; Puente-Sotomayor et al, 2021). Furthermore, the Support Vector Machine (SVM) algorithm has demonstrated excellent performance in landslide susceptibility zoning (Peng et al, 2014; Hang et al, 2015; Pham et al, 2016; Lee et al, 2017; Chen et al, 2017a; Kornejady et al, 2019; Panahi et al, 2020; Balogun et al, 2021). While landslide susceptibility assessment focuses on the spatial probability of landslide occurrence, a comprehensive landslide risk assessment requires the integration of three interrelated components: landslide hazard (probability of occurrence), elements at risk (e.g., roads, water sources, buildings, agricultural lands, electricity and telephone networks), and vulnerability of those elements (Zezere et al, 2008; Saldivar-Sali et al, 2007; Kunlong et al, 2007; Remondo et al, 2008).

Damage to building contents and vehicles on roads constitutes a major portion of landslide risk; however, evaluating these costs remains challenging due to insufficient data. Moreover, loss of human life (casualty damage) is difficult to quantify systematically (Enrique et al., 2008; Karimi Sangchini et al, 2015). The present study aims to address these gaps by conducting a comprehensive landslide risk assessment in the Varvasht Watershed. To achieve this objective, sixteen effective factors influencing landslide occurrence were identified based on local physiographic and environmental characteristics.

Materials and Methods

2.1 Study area

The Varvasht watershed is located in the northwest of Lorestan Province, Iran, within the geographical coordinates of 33°06′18″ to 33°58′19″ North latitude and 47°50′08″ to 48°41′09″ East longitude (Figure. 1). The watershed covers a total area of 15,435 hectares and constitutes a part of the Badavar and Seimareh River basins. Administratively, it lies within the jurisdiction of Nurabad City. Varowt is one of the large sub-basins of the Ghareh Su River (fourth-order watershed) and the Gazrud River (seventh-order watershed) in Delfan County. Analysis of the slope and elevation maps of the study area indicates that the minimum elevation is 1,509 meters above sea level, while the maximum elevation reaches 2,620meters. Furthermore, approximately 75% of the watershed area is characterized by slopes exceeding 15%. These topographic conditions clearly indicate the mountainous nature of the study area. Due to its steep slopes, susceptible geological formations, road construction activities, and widespread land use changes—particularly the conversion of forests and rangelands into rain-fed agricultural lands—the Varvasht watershed exhibits high susceptibility to landslide occurrence. The mean annual precipitation in the watershed is 469 mm. According to Iran's structural–tectonic divisions, the study area is situated within the Crushed (or High) Zagros structural zone. The stratigraphic units present in the study area, ranging from oldest to youngest, include lithological and sedimentary facies belonging to the Mesozoic, Cenozoic, and Quaternary eras. The predominant lithology consists of limestone, conglomerate, marl, radiolarite, and alluvial deposits. Based on field surveys and satellite data analysis, approximately 200 hectares of the watershed area are occupied by both ancient (old) and recent landslides. The land use of the watershed is predominantly rangeland and agriculture, with forest cover accounting for nearly 30% of the total area.

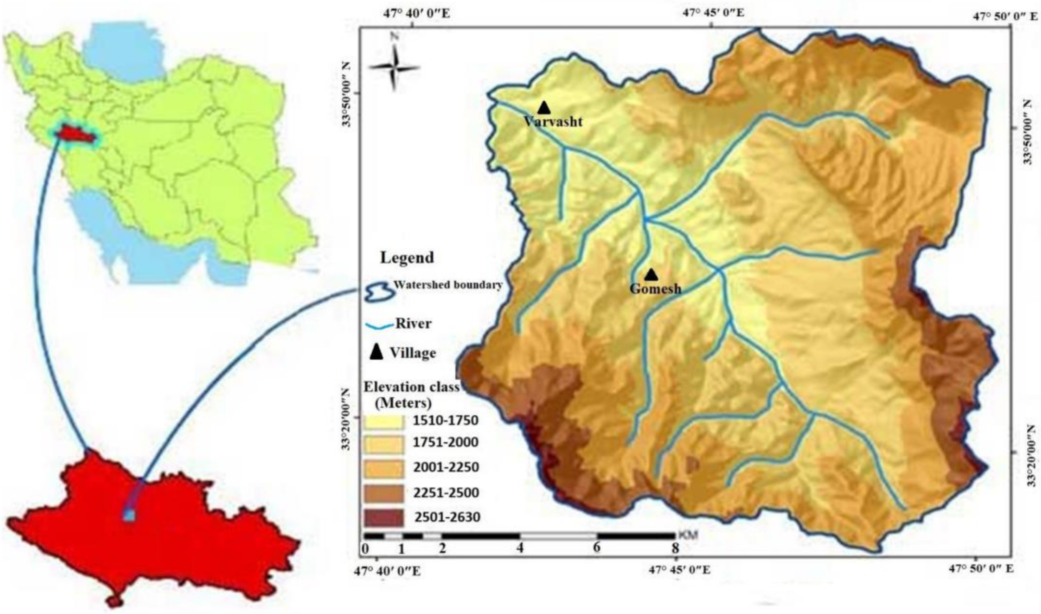

Fig. 1: Geographical site of the Varvasht Watershed

2.2 Landslide inventory map

To construct the landslide inventory map used in this study, data were collected from field works, local records, and aerial photograph interpretation. A regular sampling strategy was implemented, with one point located per 100 hectares to enable hazard assessment. A comparable number of points from stable (non-landslide) areas was also extracted to maintain a balanced representation relative to the landslide points (Figure 2).

2.3 Selection of effective factors

In the present study, a total of seventeen environmental and topographic factors were selected and analyzed as independent variables influencing landslide occurrence in the Varvasht Watershed (Mahalingam et al, 2016;

Arabameri et al, 2020a; Shano et al, 2022). The base dataset comprised a Digital Elevation Model (DEM), from which primary derivatives—including slope percentage, aspect, and stream networks—were extracted. More advanced geomorphometric indices—namely landform, the length-slope (LS) factor, Topographic Position Index (TPI), Topographic Roughness Index (TRI), and Vector Ruggedness Measure (VRM) (Figure. 8-11)—were all computed using the specialized SAGA GIS software (Tien Bui et al, 2016; Wilson et al, 2000; Hong et al, 2015; Grohmann et al, 2011; Tyagi et al, 2021; Boria et al, 2014; Kalantar et al, 2020). Distance-based layers, including distances to faults, roads, and villages, were generated through proximity analysis tools within a geographic information system environment. The geological map of the area provided lithological information for different rock units, whereas the land use map and the NDVI (Normalized Difference Vegetation Index) derived from 2025 satellite imagery reflected the respective impacts of human activities and vegetation density on slope stability. Finally, the mean annual rainfall layer was incorporated into the modeling as one of the most critical triggering factors for landslide events (Lee, 2005; Devkota et al, 2013; Lombardo et al, 2014) (Figure. 3-8). The integration of these seventeen factors yielded a comprehensive set of topographic, geological, hydrological, and anthropogenic variables, which served as the input basis for the machine learning models employed in this research (Kohavi, 1995; Václavík and Meentemeyer, 2009; Ozdemir, 2011; Chapi et al, 2017; Jebur et al, 2014; Mokarram et al, 2015).

Table 1: Summary of conditioning factors, data sources, and their roles in landslide occurrence in the Varvasht Watershed

Factor Category	Conditioning Factor	Data Source	Role in Landslide Occurrence
Topographic	Slope (%)	DEM (10 m)	Controls gravitational stress and runoff velocity
Topographic	Aspect	DEM (10 m)	Influences solar radiation and vegetation cover
Topographic	Elevation	DEM (10 m)	Affects temperature, precipitation, and vegetation
Topographic	TPI	DEM (10 m)	Identifies landform position (valley, ridge, etc.)
Topographic	TRI	DEM (10 m)	Quantifies topographic heterogeneity
Topographic	VRM	DEM (10 m)	Measures surface ruggedness
Topographic	LS factor	DEM (10 m)	Represents combined slope length and steepness
Hydrological	Topographic Wetness Index	DEM (10 m)	Indicates soil moisture distribution
Hydrological	Distance to streams	Stream network	Proximity to drainage channels
Geological	Lithology	Geological map (1:100,000)	Determines bedrock strength and weathering rate
Geological	Distance to faults	Fault map (1:100,000)	Tectonic weakness zones
Environmental	Land use	Satellite image (2025)	Reflects anthropogenic impact
Environmental	NDVI	Satellite image (2025)	Indicates vegetation density
Environmental	Annual rainfall	Meteorological stations	Primary triggering factor
Anthropogenic	Distance to roads	Topographic map (1:25,000)	Road construction effects
Anthropogenic	Distance to villages	Topographic map (1:25,000)	Population pressure

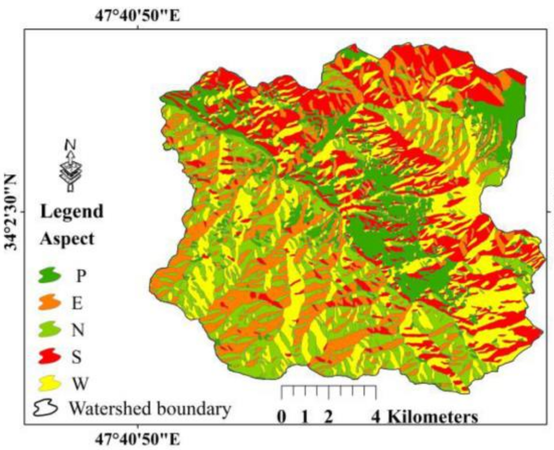

Fig. 2: Aspect map of the Varvasht Watershed

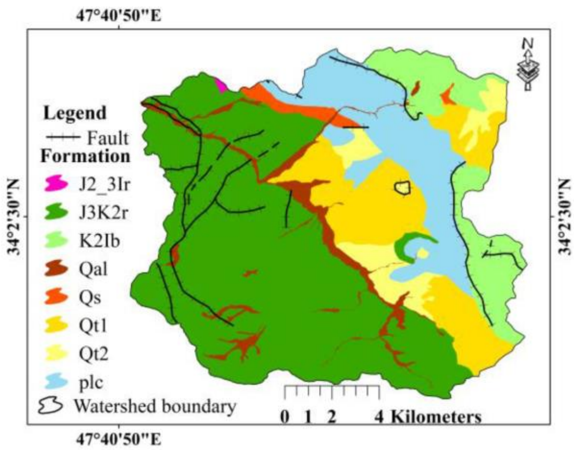

Fig. 3: Geological map of the Varvasht Watershed

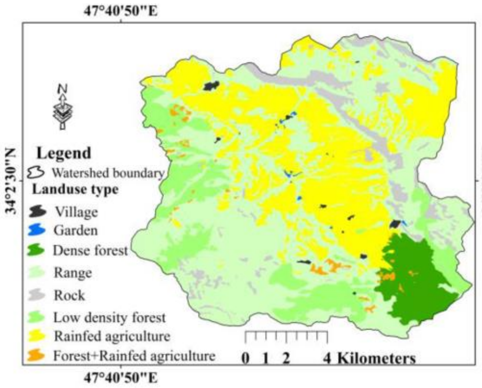

Fig. 4: Land use map of the Varvasht Watershed

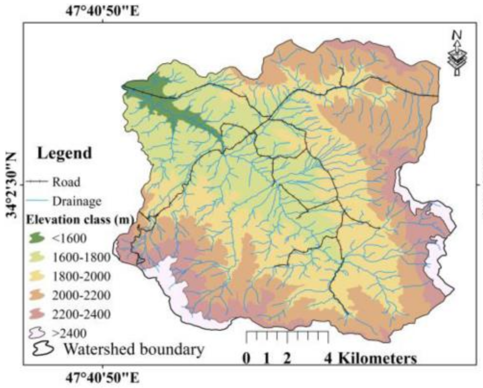

Fig. 5: Elevation map of the Varvasht Watershed overlaid with streams and roads

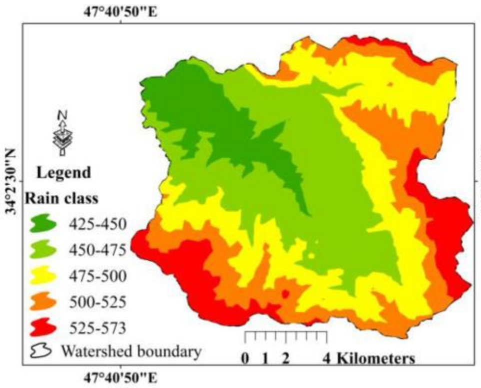

Fig. 6: Mean annual precipitation map of the Varvasht Watershed

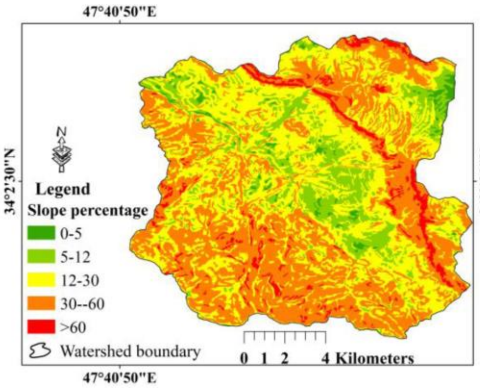

Fig. 7: Slope map of the Varvasht Watershed

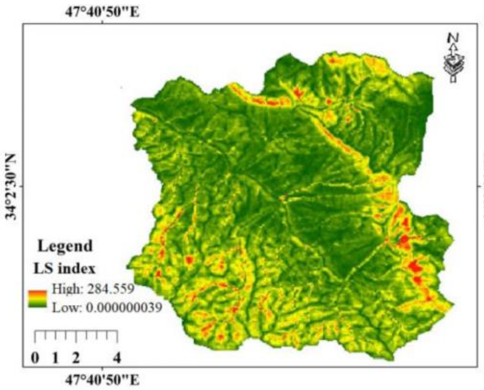

Fig. 8: LS factor map of the Varvasht Watershed

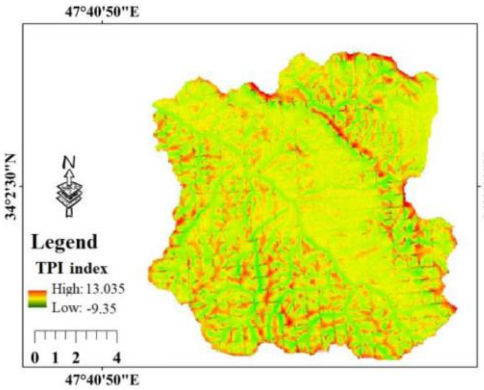

Fig. 9: TPI factor map of the Varvasht Watershed

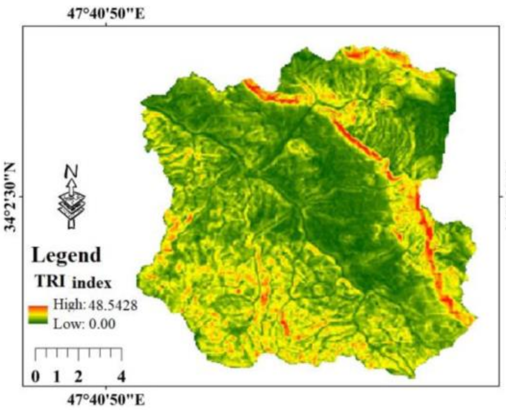

Fig. 10: TRI factor map of the Varvasht Watershed

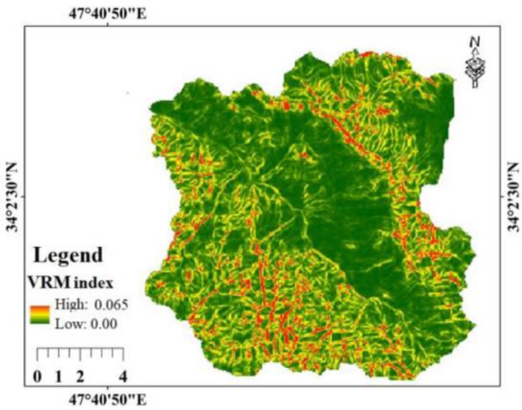

Fig. 11: VRM factor map of the Varvasht Watershed

2.4 Landslide Hazard Mapping

In the present study, landslide hazard assessment in the Varowt Watershed was conducted using three distinct machine learning models: Support Vector Machine (SVM), Generalized Linear Model (GLM), and Artificial Neural Network (ANN). Each model was applied to generate a landslide susceptibility map, which subsequently served as the hazard component in the overall landslide risk assessment framework.

Support Vector Machine (SVM) Model

The SVM algorithm is a supervised machine learning method primarily used for classification and data separation. After defining the input variables (independent factors) and target variables (dependent variable representing landslide occurrence), the SVM model analyzes the relationships between them during the calibration phase and subsequently classifies the data into distinct groups. In this algorithm, each data sample is represented as a point in an n-dimensional space, where n corresponds to the number of features associated with that sample. The value of each feature determines one coordinate component of the point on the scatter plot. The fundamental concept of SVM involves binary classification using training points, transforming the original input space into a higher-dimensional space to identify an optimal hyperplane. Training points located close to this optimal hyperplane are referred to as support vectors. Once the decision surface is established, it can be employed to estimate new, unseen data (Rabet et al, 2020). In this study, the SVM model was implemented using the SVR algorithm within ModEco software (Karimi Sangchini et al, 2024).

Generalized Linear Model (GLM)

The Generalized Linear Model extends traditional linear models to accommodate non-normal distributions. GLM consists of three components: a probability distribution for the response variable, a linear predictor, and a link function that connects the linear predictor to the mean of the distribution function (Prajisha et al, 2023). Variables in the GLM framework may be continuous, discrete, or a combination of both. In the current research, the dependent variable is binary, indicating the presence or absence of landslide occurrences. The GLM analysis in this study was performed using ModEco software. The model is expressed as follows (Prajisha et al, 2023):

Eq. 1)

$$logit(P) = \ln\left(\frac{P}{1-P}\right) = +\beta_0 + \sum_{i=1}^{n} \beta_i x_i$$

Where P represents the output probability, β_0 is the intercept factor, β_i is the coefficient of the i-th independent variable, and x_i is the i-th independent variable. The probability P can also be expressed as:

Eq. 2)

$$P = \frac{exp(\beta_0 + \sum_{i=1}^{n} \beta_i x_i)}{1 + \exp(\beta_0 + \sum_{i=1}^{n} \beta_i x_i)}$$

Artificial Neural Network (ANN) Model

In an artificial neural network, neurons are recognized as the primary processing elements that operate collectively to solve a given problem. Neurons are arranged in layers, with each network comprising an input layer and an output layer, and potentially multiple hidden layers positioned between them. Information processing occurs within the hidden layers, and the optimal number of these layers is determined through iterative experimentation to minimize error (Harmouzi et al, 2019). For ANN implementation, after initial data processing, all factor maps were converted to raster format, dividing the watershed surface into individual pixels (Sevgen et al, 2019). The number of pixels per class and the total pixel count for the watershed were extracted from the attribute tables of each factor map. In this research, a multilayer perceptron (MLP) neural network was employed, consisting of one input layer (with neurons equal to the number of selected effective factors), one hidden layer, and one output layer (with a single neuron for predicting landslide occurrence probability). The training algorithm used was backpropagation with the Adam optimizer. The ReLU (Rectified Linear Unit) activation function was applied in the hidden layer, while the sigmoid activation function was used in the output layer to generate outputs within the range [0,1] representing probability of occurrence. The number of neurons in the hidden layer was determined through a trial-and-error process combined with cross-validation. Input data (conditioning factor layers) and output data (landslide evidence map) were standardized to a common scale (Gholami and Ajallooeian, 2017). The ANN model was implemented using ModEco software.

2.5 Landslide risk map

The inventory of elements at risk in the present research included residential zones (comprising both villas and rural houses), transportation infrastructure (including asphalt and unpaved roads), land cover types (forest, rangeland, and agricultural land), and surface water resources (Zezere et al, 2008). Vulnerability scoring was conducted by considering both the presence of landslide hazard and the economic and ecological attributes of each element (Table 2). Elements situated within higher hazard categories are regarded as more critical and are therefore assigned greater vulnerability scores. The computation of vulnerability involved the integration of the inherent value of the elements at risk with the corresponding hazard class in which those elements are located (Enrique et al, 2008; Karimi Sangchini et al, 2025).

Table 2: Vulnerability core of elements at risk

Element	Factor / Type	Vulnerability Score Range
Roads	Dirt track (unpaved, no substructure); vulnerability increases by a factor of 1 with increasing hazard class	1–5
	Unpaved road with substructure; vulnerability increases by a factor of 2 with increasing hazard class	1–10
	Asphalt road with substructure; vulnerability increases by a factor of 3 with increasing hazard class	1–15
	Main road (primary road) with substructure; vulnerability increases by a factor of 4 with increasing hazard class	1–20
Residential areas	Rural residential areas; vulnerability increases by a factor of 2 with increasing hazard class	1–10
	Urban residential areas; vulnerability increases by a factor of 3 with increasing hazard class	1–15
	Tourist areas, industrial zones, mosques, fish farming workshops, post offices/banks, schools, mines, health houses; vulnerability increases by a factor of 4 with increasing hazard class	1–20
Water resources	Spring; vulnerability increases by a factor of 2 with increasing hazard intensity	1–10
	Stream (order 2); vulnerability increases by a factor of 1 with increasing hazard intensity	1–5
	Stream (order 3); vulnerability increases by a factor of 2 with increasing hazard intensity	1–10
	Stream (order 4 and above); vulnerability increases by a factor of 3 with increasing hazard intensity	1–15
	Agricultural wells and ponds; vulnerability increases by a factor of 3 with increasing hazard intensity	1–15
Agriculture	Rain-fed agricultural lands; vulnerability increases by a factor of 2 with increasing hazard intensity	1–10
	Irrigated agricultural lands; vulnerability increases by a factor of 3 with increasing hazard intensity	1–15
	Orchards (garden lands); vulnerability increases by a factor of 4 with increasing hazard intensity	1–20
Power transmission lines	Power transmission lines; vulnerability increases by a factor of 2 with increasing hazard intensity	1–10

The final step in the landslide risk assessment procedure involved the quantification of total risk using the well-established relationship originally defined by Varnes (1984). According to this relationship, risk is not a single measurable property but rather a derived quantity that integrates three essential components. The first component, hazard (H), represents the magnitude or intensity of the landslide threat. The second component, elements at risk (E), refers to the physical, social, economic, or environmental assets that are present within the hazard-prone area and could potentially experience adverse consequences. The third component, vulnerability (V), captures the susceptibility of those elements to damage, expressed as a degree of loss ranging from complete destruction (full vulnerability) to no damage (zero vulnerability). These three components are combined through a product operation, yielding the total risk value according to the equation $R = H \times E \times V$. This multiplicative approach ensures that risk is only significant when all three components are simultaneously present at non-negligible levels. After computing risk values for each spatial unit across the study area, the resulting numerical surface was classified into five qualitative classes to improve interpretability and support decision-making. The adopted classification scheme includes: very low risk, low risk, moderate risk, high risk, and very high risk.

Results and Discussion

3.1 Landslide inventory map

A prerequisite step in the present study was the preparation of a detailed landslide distribution map for the Varvasht Watershed (Figure. 12). This map was produced based on 163 landslide events that were systematically surveyed and recorded as areal (polygon) features. The total landslide-affected surface within the watershed is approximately 131.32 hectares. The smallest documented landslide covers an area of 128 m², whereas the largest landslide polygon occupies 13.32 hectares. These statistics demonstrate the considerable heterogeneity in landslide magnitude across the study area. Moreover, such a comprehensive inventory provides a robust empirical foundation for calibrating and validating the machine learning models employed in this research.

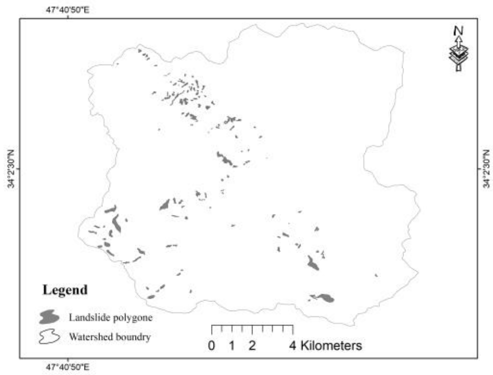

Fig. 12: Landslide distribution map in the Varvasht Watershed

3.2 Landslide hazard zonation

The final outputs obtained from the three machine learning models were used to construct landslide hazard maps. Each map was then divided into five hazard categories ranging from very low to very high risk levels. The classification scheme and the spatial distribution of hazard classes are presented in Table 3 and Figure 13, respectively.

Table 3: The scattering of area in diverse landslide hazard classes

	Generalized Linear (GLM)		Artificial Neural Network (ANN)		Support Vector Machine (SVM)	
Susceptibility class	Area (ha)	% Area	Area (ha)	% Area	Area (ha)	% Area
Very low	2982.84	19.33	6722.96	43.56	5504.31	35.66
Low	3874.70	25.10	3843.38	24.90	3492.03	22.62
Medium	3774.64	24.45	1989.94	12.89	2638.23	17.09
High	3058.91	19.82	1393.22	9.03	1957.01	12.68
Very high	1743.99	11.30	1485.59	9.62	1843.51	11.94
Total	15435.09	100	15435.09	100	15435.09	100

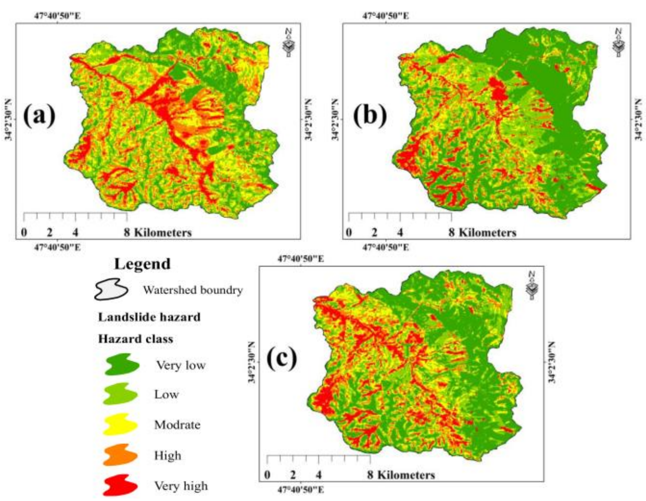

Fig. 13: Landslide hazard maps based on, a: Generalized Linear (GLM), b: Artificial Neural Network (ANN), c: Support Vector Machine (SVM)

To evaluate the predictive performance and accuracy of the models employed in this study, the Receiver Operating Characteristic (ROC) curve method and the calculation of the Area Under the Curve (AUC) were utilized. The validation results of the models are presented in Figure 14. According to the findings, the Generalized Linear Model (GLM) exhibited the lowest accuracy among the three models, with an AUC value of 0.787. The Artificial Neural Network (ANN) model demonstrated moderate performance, achieving an AUC of 0.865. In contrast, the Support Vector Machine (SVM) model attained the highest AUC value of 0.913, indicating superior predictive performance and the best capability for landslide susceptibility zonation in the Varowt Watershed. These results suggest that although all three models possess acceptable ability to identify landslide-prone areas, the SVM model significantly outperforms the other two models and can be considered the optimal model for landslide risk assessment in the study area.

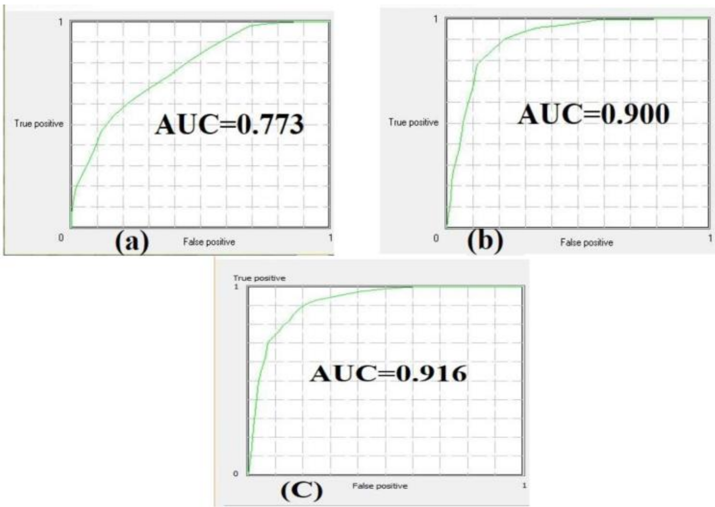

Fig. 14: ROC curves a: Generalized Linear (GLM), b: Artificial Neural Network (ANN), c: Support Vector Machine (SVM)

The results of this study demonstrated that the Support Vector Machine (SVM) model, with an Area under the Curve (AUC) value of 0.913, achieved the highest accuracy in landslide susceptibility zonation in the Varvasht Watershed. This finding is fully consistent with the results of previous studies conducted by Peng et al. (2014), Pham et al. (2016), Chen et al. (2017a), and Panahi et al. (2020), all of which introduced the SVM model as one of the most efficient machine learning algorithms for identifying landslide-prone areas. The superior performance of the SVM model can be attributed to its ability to find an optimal hyperplane for separating landslide and non-landslide data points, even in high-dimensional spaces (Rabet et al, 2020). The Artificial Neural Network (ANN) model, with an AUC value of 0.865, demonstrated moderate performance in this study. This accuracy level is somewhat lower compared to the results of studies by Chen et al. (2017a), Harmouzi et al. (2019), and Yao et al. (2022), all of which reported high performance of ANN. This discrepancy may be attributed to the topographic complexity of the study area, the number of hidden layers and neurons selected in the network architecture, as well as the volume and quality of training data (Gholami and Ajallooeian, 2017). Nevertheless, the AUC value of 0.865 still indicates the acceptable capability of this model for landslide zonation in the study area. The Generalized Linear Model (GLM), with an AUC value of 0.787, exhibited the lowest accuracy among the three models examined. This finding is somewhat different from the results of studies by Hong et al. (2015), Karimi Sangchini et al. (2016), and Abedini et al. (2017), which introduced GLM as an effective regression model. The possible reason for this relatively weaker performance may be related to the linear nature of this model and its inability to identify complex nonlinear relationships between environmental factors and landslide occurrence. As noted by Prajisha et al. (2023), despite its simplicity and high interpretability, the GLM model may perform less effectively than nonlinear models such as SVM and ANN when dealing with complex spatial patterns. The landslide hazard zonation results showed that the SVM model classified approximately 35.66% of the area as very low susceptibility, 22.62% as low, 17.09% as medium, 12.68% as high, and 11.94% as very high susceptibility. In contrast, the GLM model placed a higher percentage of the area in medium to very high susceptibility classes (totaling 55.57%) compared to the SVM model (totaling 41.71%). This difference in class area distribution indicates the more conservative approach of the SVM model in labeling areas as high susceptibility, which may result from the stricter criteria of this algorithm for data separation.

3.3 Results of landslide risk assessment

The spatial datasets required for risk assessment were compiled from various sources. Land use information, including the extent of pastures, forests, and agricultural lands, was extracted from a land use map, while spring locations were documented through field surveys.

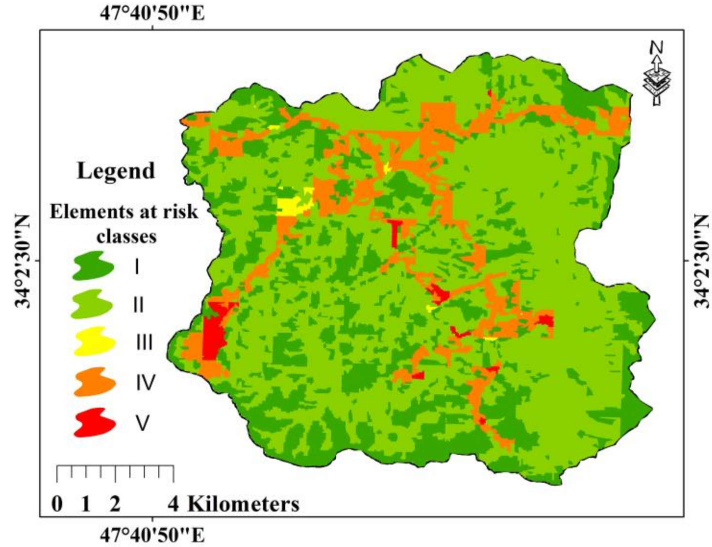

Fig. 15: Element at risk map in Varvasht Watershed

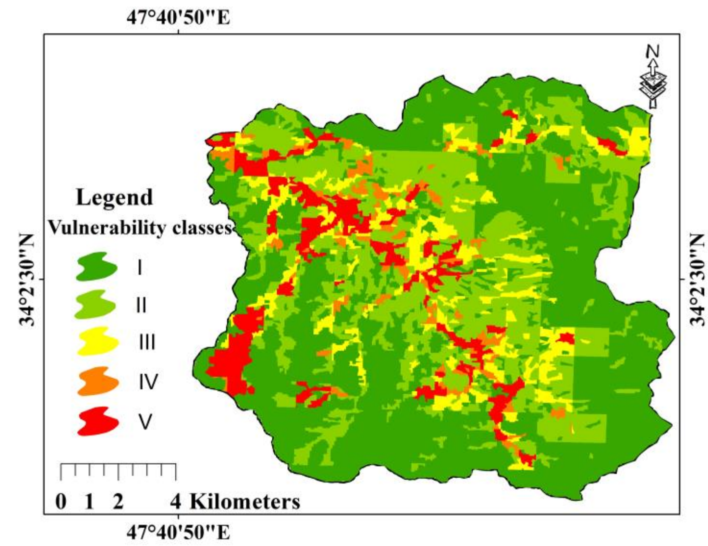

Fig. 16: Vulnerability map in Varvasht Watershed

In addition, the number and typology of residential buildings, together with the linear lengths of roads and watercourses, were obtained from a 1:25,000-scale digital topographic map. Using this information, maps of elements at risk and vulnerability were constructed. The general risk equation was subsequently applied to derive numerical risk values, which were then reclassified into five hierarchical categories: very low, low, medium, high, and very high (Table 3-6 and Figure 15-17).

Table 4: Elements at risk classes in Varvasht Watershed

classes	Number of elements	Area (ha)	% Area
Very Low	0, 1	4247.19	27.52
Low	2	9120.77	59.09
Medium	3	71.77	0.46
High	4	1809.31	11.72
Very High	5	186.06	1.21
Total		15435.09	100

Table 5: Vulnerability classes in Varvasht Watershed

classes	Vulnerability number	Area (ha)	% Area
Very low	0.0-15	7804.41	50.56
Low	16-30	4596.19	29.78
Medium	31-45	1351.08	8.75
High	46-60	509.11	3.30
Very high	61-75	1174.29	7.61
Total		15435.09	100

In the risk assessment section, the integration of the hazard map (using the best model, i.e., SVM), the elements at risk map, and the vulnerability map produced the final risk map. The results indicated that approximately 54.86% of the watershed falls within the very low-risk class, 26.08% in the low-risk class, 10.84% in the medium-risk class, 4.28% in the high-risk class, and 3.94% in the very high-risk class. Overall, about 19% of the area (equivalent to 2,968 hectares) is classified as high and very high-risk classes, necessitating prioritization in management and mitigation measures.

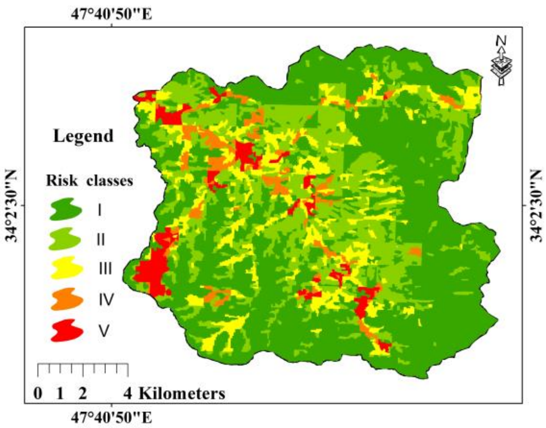

Fig. 17: Risk map in Varvasht Watershed

Table 6: The delivery of zone in diverse landslide risk classes

class	Pixel value	Area (ha)	% Area
Very low	0-25	8467.17	54.86
Low	26-50	4026.20	26.08
Medium	51-75	1673.40	10.84
High	76-100	660.43	4.28
Very high	101-125	607.90	3.94
Total		15435.09	100

Comparison of the elements at risk and vulnerability maps revealed that although the largest area of the watershed (approximately 59%) falls within the low vulnerability class, areas with high and very high vulnerability classes (totaling about 11%) largely overlap with areas of high hazard classes. This overlap, which is also reflected in the final risk map, further emphasizes the importance of an integrated risk assessment approach (combining hazard, elements at risk, and vulnerability) (Zezere et al, 2008; Enrique et al, 2008). Based on the findings of this study and with reference to previous research, it can be concluded that the use of machine learning models, particularly SVM, combined with accurate identification of elements at risk and determination of their vulnerability degree, constitutes an effective and efficient approach for landslide risk assessment in mountainous regions (Carrara et al, 2003; Dahal et al, 2008; Kayastha et al, 2013). This approach can serve as a model for other areas with similar physiographic and climatic conditions in Iran and worldwide. The spatial datasets required for risk assessment were compiled from various sources. Land use information, including the extent of pastures, forests, and agricultural lands, was extracted from a land use map, while spring locations were documented through field surveys. In addition, the number and typology of residential buildings, together with the linear lengths of roads and watercourses, were obtained from a 1:25,000-scale digital topographic map. Using this information, maps of elements at risk and vulnerability were constructed. The general risk equation was subsequently applied to derive numerical risk values, which were then reclassified into five hierarchical categories: very low, low, medium, high, and very high (Fig. 7, Table 6). The spatial distribution of the final risk map (Fig. 7) reveals a clear and consistent pattern of high and very high-risk zones, which are predominantly concentrated in specific geomorphic and geological settings. A detailed overlay analysis of the risk map with the geological layer (Fig. 1) indicates that nearly 68% of the high-risk areas (approximately 2,018 ha) are located on geological formations belonging to the Mesozoic era, particularly the radiolarite and marl units. These lithological units are characterized by high weathering rates, low shear strength, and impermeable layers, which facilitate the development of failure planes under saturated conditions. In contrast, areas underlain by massive limestone and Quaternary alluvial deposits (mainly in the northern and central low-relief plains) fall predominantly within very low to low-risk classes, confirming the controlling role of lithology in slope instability. Furthermore, the intersection of the risk map with landform classes derived from the Topographic Position Index (TPI) demonstrates that high-risk zones are overwhelmingly associated with valley floors, steep side-slopes, and convex footslopes. These landforms act as natural accumulation zones for colluvial materials and surface runoff, exacerbating pore-water pressure and reducing slope stability. Conversely, ridge tops and gentle planar slopes exhibit minimal landslide risk, which aligns with the findings of previous studies in similar mountainous terrains (Karimi Sangchini et al, 2016; Arabameri et al, 2020). In terms of drainage network proximity, approximately 43% of the high and very high-risk areas (about 1,276 ha) are located within a 100-meter buffer zone of second- and third-order streams. This spatial correlation is attributed to the combined effects of bank undercutting, elevated soil moisture content, and seasonal fluctuations in groundwater levels, which are well-documented triggering mechanisms for shallow landslides in the Zagros region. Additionally, the density of the drainage network in high-risk zones is significantly higher (2.8 km/km²) compared to low-risk zones (1.2 km/km²), further emphasizing the role of hydrological processes in landslide occurrence. Slope angle analysis reveals that more than 75% of the high-risk areas occur on slopes exceeding 25°. This threshold aligns with the critical slope angle reported for similar lithological and climatic conditions (Lee and Pradhan, 2007; Pourghasemi and Rahmati, 2018). The combination of steep slopes with marl and radiolarite lithologies creates a highly unstable environment, where even moderate rainfall events can trigger mass movements. The high-risk zones are also characterized by a southwest-facing aspect, which receives higher solar radiation, leading to increased freeze-thaw cycles and mechanical weathering of rock units. Another striking observation is the coincidence of high-risk zones with areas of intensive anthropogenic intervention. Overlaying the risk map with land use and road networks shows that approximately 34% of the high-risk areas are located within 200 meters of main roads and unpaved rural tracks. Road construction has not only altered natural drainage patterns but also created over-steepened cut slopes that are highly susceptible to failure. Similarly, the conversion of natural forests and rangelands into rain-fed agricultural lands—particularly on slopes with gradients between 20° and 30°—has accelerated soil erosion and reduced slope stability, as reflected in the clustering of high-risk pixels in these agricultural patches. In summary, the spatial coincidence of high-risk zones with radiolarite-marl formations, valley-floor landforms, dense drainage networks (especially near 2nd- and 3rd-order streams), and steep slopes (> 25°), along with anthropogenic stressors such as road construction and agricultural expansion, collectively explains the elevated risk levels in the Varvasht Watershed. This multi-factor spatial analysis not only validates the predictive performance of the SVM-based hazard map but also provides actionable insights for targeted mitigation planning.

Conclusion

The present study was conducted with the aim of comprehensive landslide risk assessment in the Varvasht Watershed, Lorestan Province, using three machine learning models: Generalized Linear Model (GLM), Artificial Neural Network (ANN), and Support Vector Machine (SVM). Based on the integration of the SVM-generated hazard map with elements at risk and their vulnerability, the following conclusions can be drawn:

4.1. Model performance and methodological implications

The comparative evaluation of the three models revealed that the SVM algorithm (AUC = 0.913) significantly outperformed ANN (AUC = 0.865) and GLM (AUC = 0.787) in predicting landslide susceptibility. This superior performance is attributable to the kernel-based nature of SVM, which effectively captures complex, non-linear interactions among the seventeen effective factors—a critical advantage in geomorphologically complex terrains where linear assumptions (as in GLM) are inherently violated. The moderate performance of ANN, despite its non-linear capability, may be related to the limited number of training samples (163 landslide polygons) and the difficulty in optimizing network architecture for small-to-medium datasets. These findings underscore that, for mountainous regions with similar data constraints, kernel-based algorithms like SVM offer a more reliable and robust approach for susceptibility mapping compared to conventional regression techniques or black-box neural networks.

4.2. Spatial patterns and geo-environmental controls

The spatial analysis of the final risk map (Section 3.3) demonstrated that high and very high-risk zones (totaling 2,968 ha, approximately 19% of the watershed) are not randomly distributed but are systematically associated with specific geo-environmental conditions. The convergence of high-risk areas with radiolarite and marl formations (68% overlap), slopes exceeding 25° (75% overlap), valley-floor landforms, and proximity to 2nd- and 3rd-order streams (43% within a 100-m buffer) indicates a multi-causal cascade of instability. Lithological weakness (low shear strength and high weathering rates) provides the intrinsic susceptibility, while steep slopes and hydrological concentration (stream proximity and elevated soil moisture) act as extrinsic triggers. The additional coincidence of high-risk zones with road networks (34% within 200 m) and rain-fed agricultural lands (30% overlap) further highlights the synergistic role of anthropogenic disturbances—road construction altering natural drainage and agricultural expansion accelerating soil degradation—in exacerbating the inherent natural hazard. This spatial diagnostic confirms that landslide risk in the Varvasht Watershed is not a mono-causal phenomenon but rather the product of coupled natural-human systems.

4.3. Management and mitigation implications

The findings carry direct and actionable implications for sustainable land-use planning and disaster risk reduction in the Varvasht Watershed and analogous regions in the Zagros Mountains: Priority intervention zones: The 2,968 ha classified as high and very high risk should be designated as "No-Go Zones" for new residential or infrastructure development. Existing linear infrastructure (roads and power lines) traversing these zones require immediate engineering assessment, including the installation of retaining walls, surface drainage systems, and slope stabilization measures (e.g., soil nailing or vegetation reinforcement). Land-use regulation: The strong association between agricultural expansion and high-risk zones (30% overlap) necessitates strict enforcement of slope-based land-use zoning. Rain-fed cultivation on slopes exceeding 20° should be progressively discouraged through incentive-based programs promoting terracing, agroforestry, or conversion to permanent grassland. Early warning and community preparedness: The spatial predictability of high-risk zones (based on lithology, slope, and stream proximity) enables the design of a targeted early warning system. Rainfall thresholds for landslide initiation should be established for these geologically sensitive areas, and local communities should be trained in evacuation protocols and landslide recognition. Road maintenance protocol: Given that 34% of high-risk zones fall within 200 m of roads, a routine inspection and maintenance program for road cuts, culverts, and drainage ditches should be institutionalized, particularly before and during the wet season (November to April).

4.4. Limitations and directions for future research

Despite the robust performance of the SVM model and the comprehensive risk assessment framework, several limitations should be acknowledged. First, the vulnerability scoring, although based on expert judgment (Delphi method), remains subjective and could be refined through economic valuation of assets and probabilistic damage curves. Second, the temporal dimension of risk (i.e., probability of occurrence within a specific time window) was not addressed; future studies should integrate rainfall frequency analysis and climate change scenarios to produce dynamic risk maps. Third, the casualty component (human fatalities) was not quantified due to the absence of reliable historical data on landslide-related deaths in the study area; developing a systematic database for human losses is a critical priority for future research. Fourth, while the SVM model performed best among the three algorithms tested, exploring ensemble methods (e.g., Random Forest combined with SVM) and deep learning architectures (e.g., Convolutional Neural Networks) may further enhance predictive accuracy, especially as more training data become available.

4.5. Concluding remarks

In summary, this study demonstrates that the integration of SVM-based susceptibility mapping with spatially explicit elements at risk and vulnerability assessment, according to the R = H × E × V framework, provides a scientifically robust and operationally applicable methodology for landslide risk assessment in data-scarce, mountainous environments. The spatial diagnosis of high-risk zones, linked to specific lithological, geomorphological, and anthropogenic drivers, offers a transparent and evidence-based foundation for targeted mitigation strategies. The approach presented here can serve as a replicable model for other watersheds in Iran and similar physiographic regions worldwide, contributing to the broader goals of sustainable development and disaster resilience in landslide-prone areas.

Acknowledgment

This article has been done in the procedure of a research project between the Soil Conservation and Watershed Management Research Institute and the Agricultural and Natural Resources Research Center of Lorestan Province with the number 2-59-29-021-020693. It is necessary to express our sincere gratitude for the collaboration of these centers in all stages of the project. This project was funded under the project entitled "Assessment of Landslide Risk Damage in the Varvasht Watershed, Lorestan Province". We would like to thank the Soil Conservation and Watershed Management Research Office for their support. The authors have no conflict of interests whatsoever.

References

Abedini, M., Ghasemyan, B. and Rezaei Mogaddam, M.H., (2017) Landslide susceptibility mapping in Bijar city, Kurdistan Province, Iran: a comparative study by logistic regression and AHP models, Environmental earth sciences, v. 76(8), p. 1-14.

Aghda, S.F, Bagheri, V. and Razifard, M., 2018. Landslide susceptibility mapping using fuzzy logic system and its influences on mainlines in lashgarak region, Tehran, Iran, Geotechnical and Geological Engineering, v. 36, p. 915-937.

Aleotti, P. and Chowdhury, R., 1999. Landslide hazard assessment: summary review and new perspectives, Bull Eng Geol Environ, v. 58, p. 21-44.

Arabameri, A., Karimi Sangchini, E., Pal, S.C., Saha, A., Chowdhuri, I., Lee, S. and Tien Bui, D., 2020a. Novel Credal Decision Tree-Based Ensemble Approaches for Predicting the Landslide Susceptibility, Remote Sensing, v. 12, p. 3389. https://doi.org/10.3390/rs12203389.

Arabameri, A., Saha, S., Roy, J., Chen, W., Blaschke, T. and Tien Bui, D., 2020b. Landslide Susceptibility Evaluation and Management Using Different Machine Learning Methods in the Gallicash River Watershed, Iran, Remote Sensing, v. 12, 475 p.

Balogun, A.L., Rezaie, F., Pham, Q.B., Gigović, L., Drobnjak, S., Aina, Y.A., Panahi, M., Temitope, S. and Yekeen, S.L., 2021. Spatial prediction of landslide susceptibility in western Serbia using hybrid support vector regression (SVR) with GWO, BAT and COA algorithms, Geoscience Frontiers, v. 12(3), p. 101104. https://doi.org/10.1016/j.gsf.2020.10.009.

Barman, J., Ali, S.S., Biswas, B. and Das, J., 2023. Application of index of entropy and Geospatial techniques for landslide prediction in Lunglei district, Mizoram, India, Natural Hazards

Research https://doi.org/10.1016/j.nhres.2023.06.006.

Bathrellos, G.D., Kalivas, D.P. and Skilodimou, H.D., 2009. GIS-based landslide susceptibility mapping models applied to natural and urban planning in Trikala, Central Greece, Estudios Geológicos, v. 65(1), p. 49-65. doi:10.3989/egeol.08642.036.

Boria, R.A., Olson, L.E., Goodman, S.M. and Anderson, R.P., 2014. Spatial filtering to reduce sampling bias can improve the performance of ecological niche models, Ecological Modelling, v. 275, p. 73-77.

Burak, F.T., Abbaspour, A., Alimohammadlou, Y. and Tecuci, G., 2021. Landslide susceptibility analyses using Random Forest, C4.5, and C5.0 with balanced and unbalanced datasets, Catena, v. 203, p. 105355, https://doi.org/10.1016/j.catena.2021.105355.

Carrara, A., Giovanni, C. and Frattini, P., 2003. Geomorphological and historical data in assessing landslide hazard, Earth Surface Processes and Landforms, v. 28, p. 1125-1142. doi:10.1002/esp.545.

Chapi K, Singh VP, Shirzadi A, Shahabi H, Bui DT, Pham BT, Khosravi K (2017) A novel hybrid artificial intelligence approach for flood susceptibility assessment, Environmental Modelling and Software, v. 95, p. 229-245.

Chen, W., Pourghasemi, H.R., Kornejady, A. and Zhang, N., 2017a. Landslide spatial modeling: Introducing new ensembles of ANN, MaxEnt, and SVM machine learning techniques, Geoderma, v. 305, p. 314-327.

Chen, W., Xie, X., Wang, J., Pradhan, B., Hong, H., Bui, D.T., Duan, Z. and Ma, J., 2017b. A comparative study of logistic model tree, random forest and classification and regression tree models for spatial prediction of landslide susceptibility, Catena, v. 151, p. 147-160.

Chen, W., Yan, X., Zhao, Z., Hong, H., Bui, D.T. and Pradhan, B., 2019. Spatial prediction of landslide susceptibility using data mining-based kernel logistic regression, naive Bayes and RBFNetwork models for the Long County area (China), Bulletin of Engineering Geology and the Environment, v. 78, p. 247-266.

Convertino, M., Troccoli, A. and Catani, F., 2013. Detecting fingerprints of landslide drivers: a MaxEnt model, Journal of Geophysical Research: Earth Surface, v. 118(3), p. 1367-1386.

Dahal, R.K., Hasegawa, S., Nonomura, S., Yamanaka, M., Masuda, T. and Nishino, K., 2008. GIS-based weights-of-evidence modelling of rainfall-induced landslides in small catchments for landslide susceptibility mapping, Environmental Geology, v. 54, p. 311-324.

Devkota, K., Regmi, A., Pourghasemi, H.R., Yoshida, K., Pradhan, B., Ryu, I., Dhital, M. and Althuwaynee, Q., 2013. Landslide susceptibility mapping using certainty factor, index of entropy and logistic regression models in GIS and their comparison at Mugling–Narayanghat road section in Nepal Himalaya, Nat Hazards, v. 65, p. 135-165.

Grohmann, C.H., Smith, M.J. and Riccomini, C., 2011. Multi-scale Analysis of Topo- graphic Surface Roughness in the Midland Valley, Scotland, IEEE Transactions on Geoscience and Remote Sensing, v. 49, p. 1200-1213. DOI:10.1109/TGRS.2010.2053546

Harmouzi, H., Nefeslioglu, H.A., Rouai, M., Sezer, E.A., Dekayir, A. and Gokceoglu, C., 2019. Landslide susceptibility mapping of the Mediterranean coastal zone of Morocco between Oued Laou and El Jebha using artificial neural networks (ANN), Arabian Journal of Geosciences, v. 12(22), p. 1-18.

Hemasinghe, H., Rangali, R.S., Deshapriya, N.L. and Samarakoon, L., 2018. Landslide susceptibility mapping using logistic regression model (a case study in Badulla District, Sri Lanka), Procedia engineering, v. 212, p. 1046-1053.

Hong, H., Pradhan, B., Xu, C. and Bui, D.T., 2015. Spatial prediction of landslide hazard at the Yihuang area (China) using two-class kernel logistic regression, alternating decision tree and support vector machines, Catena, v. 133, p. 266-281.

Jebur, M.N., Pradhan, B. and Tehrany, M.S., 2014. Optimization of landslide conditioning factors using very high-resolution airborne laser scanning (LiDAR) data at catchment scale, Remote Sensing Environmental, v. 152, p. 150-165.

Kalantar, B., Ueda, N., Saeidi, V., Ahmadi, K., Halin, A.A. and Shabani, F., 2020. Landslide Susceptibility Mapping: Machine and Ensemble Learning Based on Remote Sensing Big Data, Remote Sensing, v. 12, p. 1737.

Karimi Sangchini, E., Ownegh, M., Sadoddin, A. and Mashayekhan, A., 2011. Probabilistic Landslide Risk Analysis and Mapping (Case Study: Chehel-Chai watershed, Golestan Province, Iran), Journal of Rangeland Science, v. 2(1), p. 425-436.

Karimi Sangchini, E., Arami, S., Rezaii Moghadam, H., Khodabakhshi, Z. and Jafari, R., 2015. Landslide Risk Assessment for Baba Heydar Watershed, Chaharmahal and Bakhtiari Province, Iran, Iranian journal of earth sciences, v. 6(2), p. 121-132.

Karimi Sangchini, E., Emami, S., Tahmasebipour, N., Pourghasemi, H., Naghibi, S.A., Arami, S. and Pradhan, B., 2016. Assessment and comparison of combined bivariate and AHP models with logistic regression for landslide susceptibility mapping in the Chaharmahal-e-

Bakhtiari Province, Iran, Arabian journal of geosciences, v. 9(201), p. 1-15.

Karimi Sangchini, E., Salehpour Jam, A. and Mosaffaie, J., 2022. Flood risk management in Khorramabad watershed using the DPSIR framework, Natural Hazards, v. 122(1), p. 3101-3121.

Karimi Sangchini, E., Arami, S.H. and Dastranj, A., 2024. Accuracy assessment of GLM and SVM models in preparing a landslide susceptibility map (Case study: Karganeh watershed, Lorestan province). Researches in Earth Sciences, v. 15(3), p. 119-136 (In Persian).

Karimi Sangchini, E., Arami, S.H. and Dastranj, A., 2025. Preparation of landslide risk map in Karganeh Watershed, Lorestan Province, Iran. International Journal of Mining and Geo-Engineering, v. 59(3), p. 211-220.

Karimi Sangchini, E., Arami, S.H., Dehghani, R., Dastranj, A., Zand, M. and Bahadori, M., 2026. Assessment of the Economic, Social, and Environmental Impacts of Drought on the Stakeholders of the Karganeh Watershed in Iran. Environmental Resources Research, Doi: 10.22069/ijerr.2026.23957.1543

Kayastha, P., Dhital, M.R. and De Smedt, F., 2013. Evaluation and comparison of GIS based landslide susceptibility mapping procedures in Kulekhani watershed, Nepal, Journal of the Geological Society of India, v. 81, p. 219-231.

Kelarestaghi, A. and Ahmadi, H., 2009. Landslide susceptibility analysis with a bivariate approach and GIS in Northern Iran. Arabian journal of geosciences, v. 2, p. 95-101.

Kerekes, A., Poszet, S. and Gal, A., 2018. Landslide susceptibility assessment using the maximum entropy model in a sector of the Cluj–Napoca Municipality, Romania, Revista de Geomorfologie, v. 20(1), p. 130-146.

Kim, H.G., Lee, D.K., Park, C., Kil, S., Son, Y. and Park, J.H., 2015. Evaluating landslide hazards using RCP 4.5 and 8.5 scenarios, Environmental earth sciences, v. 73(3), p. 1385-1400.

Kohavi, R., 1995. A study of cross-validation and bootstrap for accuracy estimation and model selection, In Proceedings of the International Joint Conference on Artifcial Intelligence (IJCAI), Montreal, QC, Canada, v. 20-25(14), p. 1137-1145.

Kornejady, A., Pourghasemi, H.R. and Afzali, S.F., 2019. Presentation of RFFR new ensemble model for landslide susceptibility assessment in Iran, In Landslides: theory, practice and modelling, p. 123-143.

Kunlong, Y.I.N., Lixia, C.H.E.N. and Zhang, G., 2007. Regional landslide hazard warning and risk assessment. Earth Science Frontiers, v. 14(6), p. 85-93.

Lee, S., 2005. Application of logistic regression model and its validation for landslide susceptibility mapping using GIS and remote sensing data, International Journal of Remote Sensing, v. 26(7), p. 1477-1491.

Lee, S., Hong, S.M. and Jung, H.S., 2017. A support vector machine for landslide susceptibility mapping in Gangwon Province, Korea, Sustainability, v. 9(1), 48 p.

Lombardo, L., Cama, M., Maerker, M. and Rotigliano, E., 2014. A test of transferability for landslides susceptibility models under extreme climatic events: Application to the Messina 2009 disaster, Natural Hazards, v. 74, p. 1951-1989.

Mahalingam, R., Olsen, M.J. and O'Banion, M.S., 2016. Evaluation of landslide susceptibility mapping techniques using lidar-derived conditioning factors (Oregon case study), Geomatics, Natural Hazards and Risk, v. 7, p. 1884-1907.

Mokarram, M., Roshan, G. and Negahban, S., 2015. Landform classification using topography position index (Case study: Salt dome of Korsia-Darab plain, Iran), Modeling Earth Systems and Environment, v. 1, p.40.

Oh, H.J. and Lee, S., 2017. Shallow landslide susceptibility modeling using the data mining models artificial neural network and boosted tree. Applied Sciences, v. 7, p. 1000.

Ozdemir, A., 2011. Using a binary logistic regression method and GIS for evaluating and mapping the groundwater spring potential in the Sultan Mountains (Aksehir, Turkey), Journal of Hydrology, v. 405, p. 123-136.

Panahi, M., Gayen, A., Pourghasemi, H.R., Rezaie, F. and Lee, S., 2020. Spatial prediction of landslide susceptibility using hybrid support vector regression (SVR) and the adaptive neuro-fuzzy inference system (ANFIS) with various metaheuristic algorithms, Science of The Total Environment, v. 741, 139937. https://doi.org/10.1016/j.scitotenv.2020.139937.

Pandey, V.K., Pourghasemi, H.R. and Sharma, M.C., 2020. Landslide susceptibility mapping using maximum entropy and support vector machine models along the Highway Corridor, Garhwal Himalaya, Geocarto International, v. 35(2), p. 168-187.

Park, N.W., 2015. Using maximum entropy modeling for landslide susceptibility mapping with multiple geo environmental data sets, Environmental Earth Sciences, v. 73(3), p. 937-949.

Peng, L., Niu, R., Huang, B., Wu, X., Zhao, Y. and Ye, R., 2014. Landslide susceptibility mapping based on rough set theory and support vector machines: A case of the Three Gorges area, China, Geomorphology, v. 204, p. 287-301.

Pham, B.T., Pradhan, B., Bui, D.T., Prakash, I. and Dholakia, M.B., 2016. A comparative study of different machine learning methods for landslide susceptibility assessment: A case study of

Uttarakhand area (India), Environmental Modelling and Software, v. 84, p. 240-250.

Pham, B.T., Prakash, I., Singh, S.K., Shirzadi, A., Shahabi, H., Tran, T.T.T. and Bui, D.T., 2019. Landslide susceptibility modeling using Reduced Error Pruning Trees and different ensemble techniques: Hybrid machine learning approaches, Catena, v. 175, p. 203-218.

Phillips, S.J., Anderson, R.P. and Schapire, R.E., 2006. Maximum entropy modeling of species geographic distributions, Ecological modelling, v. 190(3), p. 231-259.

Pontius, R.J. and Schneider, L.C., 2001. Land-cover change model validation by an ROC method for the Ipswich watershed, Massachusetts, USA, Agriculture, Ecosystems and Environment, v. 85, p. 239-248.

Pourghasemi, H.R. and Rahmati, O., 2018. Prediction of the landslide susceptibility: Which algorithm, which precision? Catena, v. 162, p. 177-192.

Puente-Sotomayor, F., Mustafa, A. and Teller, J., 2021. Landslide Susceptibility Mapping of Urban Areas: Logistic Regression and Sensitivity Analysis applied to Quito, Ecuador, Geo environmental Disasters, v. 8(1), p. 1-26.

Qian, H., Wang, M. and Liu, K., 2021. Rapidly assessing earthquake-induced landslide susceptibility on a global scale using random forest, Geomorphology, v. 391, p. 107889. https://doi.org/10.1016/j.geomorph.2021.107889.

Rahmati, O., Kornejady, A., Samadi, M., Nobre, A.D. and Melesse, A.M., 2018. Development of an automated GIS tool for reproducing the HAND terrain model, Environmental modelling and software, v. 102, p. 1-12.

Regmi, A.D., Chandra Devkota, K., Yoshida, K., Pradhan, B., Pourghasemi, H.R., Kumamoto, T. and Akgun, A., 2013. Application of frequency ratio, statistical index, and weights-of-evidence models and their comparison in landslide susceptibility mapping in Central Nepal Himalaya, Arabian Journal of Geosciences, v. 7(2), p. 725-742.

Remondo, J., Bonachea, J. and Cendrero, A., 2008. Quantitative landslide risk assessment and mapping on the basis of recent occurrences. Geomorphology, v. 94(3-4), p. 496-507.

Saldivar-Sali, A. and Einstein, H.H., 2007. A landslide risk rating system for Baguio, Philippines. Engineering Geology, v. 91(2), p. 85-99.

Sevgen, E., Kocaman, S., Nefeslioglu, H.A. and Gokceoglu, C., 2019. A novel performance assessment approach using photogrammetric techniques for landslide susceptibility mapping with logistic regression, ANN and random forest, Sensors, v. 19(18), p. 3940.

Shano, L., Raghuvanshi, T.K. and Meten, M., 2021. Landslide Hazard Zonation using Logistic Regression Model: The Case of Shafe and Baso Catchments, Gamo Highland, Southern Ethiopia, Geotechnical and Geological Engineering, p. 1-19.

Sun, D., Xu, J., Wen, H. and Wang, D., 2021. Assessment of landslide susceptibility mapping based on Bayesian hyperparameter optimization: A comparison between logistic regression and random forest, Engineering Geology, v. 281, p. 105972.

Tien Bui, D., Ho, T.C., Pradhan, B., Pham, B.T., Nhu, V.H. and Revhaug, I., 2016. GIS-based modeling of rainfall-induced landslides using data mining-based functional trees classifier with AdaBoost, Bagging, and MultiBoost ensemble frameworks, Environmental Earth Sciences, v. 75, 1101 p.

Tyagi, A., Tiwari, R.K. and James, N., 2021. GIS-Based Landslide Hazard Zonation and Risk Studies Using MCDM. In Local Site Effects and Ground Failures, Springer Singapore, p. 251-266.

Václavík, T. and Meentemeyer, R.K., 2009. Invasive species distribution modeling (iSDM): Are absence data and dispersal constraints needed to predict actual distributions? Ecological Modelling, v. 220, p. 3248-3258.

Varnes, D.J., 1984. Landslide hazard zonation: A review of Principes and Practice, UNESCO, France, 63 p.

Wilson, J.P. and Gallant, J.C., 2000. Terrain Analysis: Principles and Applications; John Wiley & Sons: Hoboken, NJ, USA; 524 p.

Yao, J., Qin, S., Qiao, S., Liu, X. and Zhang, C.J., 2022. Application of a two-step sampling strategy based on deep neural network for landslide susceptibility mapping, Bulletin of Engineering Geology and the Environment, v. 81(4), p. 1-20.

Zezere, J.L., Garcia, R.A.C., Oliveria, S.C. and Reis, E., 2008. Probabilistic landslide risk analysis considering direct costs in the area north of Lisbon (Portugal). Geomorphology, v. 94, p. 467-495.

Zhao, L., Wu, X., Niu, R., Wang, Y. and Zhang, K., 2020. Using the rotation and random forest models of ensemble learning to predict landslide susceptibility, Geomatics, Natural Hazards and Risk, v. 11(1), p. 1542-1564.

Zhou, X., Wen, H., Zhang, Y., Xu, J. and Zhang, W., 2021. Landslide susceptibility mapping using hybrid random forest with GeoDetector and RFE for factor optimization, Geoscience Frontiers, v. 12(5), p. 101211.